PCCP

View Online
Dynamic Article Links

Cite this: *Phys. Chem. Chem. Phys.*, 2011, **13**, 15283–15290

www.rsc.org/pccp

PAPER

Experimental and theoretical study of the metastable decay of negatively charged nucleosides in the gas phase†

Helga Dögg Flosadóttir, Hannes Jónsson, Snorri Th. Sigurdsson and Oddur Ingólfsson*

Received 23rd April 2011, Accepted 24th June 2011
DOI: 10.1039/c1cp21298b

Fragmentation of metastable anions of all deoxynucleosides and nucleosides constituting DNA and RNA has been studied experimentally and by computer simulations. The ions were formed through deprotonation in matrix assisted laser desorption/ionisation (MALDI). Clear difference in fragmentation patterns was obtained for nucleosides containing purine *vs.* pyrimidine bases. To elucidate the role of various potential deprotonation sites, systematic blocking by chemical modification was performed and this gave unambiguous correlation between deprotonation sites and fragments observed. Classical dynamics simulations of the fragmentation process, using density functional theory to describe the electronic degrees of freedom, were performed for the various deprotonation sites. These were found to reproduce the observed fragmentation patterns remarkably well.

Introduction

Reaction and dissociation mechanisms of ions in solutions have been of interest to chemists for centuries. These reactions mainly occur from the electronic ground state of the ions and generally are rare events compared with the time scale of vibrations.[1] Unimolecular dissociation of isolated ions in the gas phase, on the other hand, is commonly induced by electronic excitation and often proceeds directly from a dissociative state. It is, however, well known that even though the initial fragmentation of an ion created through electron bombardment or photo-excitation may proceed from an electronically excited state, the excited ion can convert its electronic energy to vibrational energy and further statistical fragmentation commonly occurs.[2,3] Such unimolecular fragmentation induced by electron bombardment has been widely used to identify new synthetic compounds and compounds with previously unknown structures. Similar approaches are currently applied in tandem mass spectrometry for the characterization and identification of complex bio-molecules.[4,5] After collisional activation and subsequent parent or primary fragment ion preselection, the products of their further fragmentation are analysed. Such fragmentation processes are commonly monitored within a time window of several micro seconds, hence within the time window of metastable decay. Low energy electrons in the energy range from about 0–10 eV are also known to induce fragmentation efficiently and selectively, even though their energy is well below the ionisation limit. Such dissociative electron attachment (DEA) proceeds through a resonant vertical transition from the ground state of the neutral to a corresponding negative ion state. The so formed transient negative ion (TNI) may be in its electronic ground state or an excited state, depending on the nature of the transition, and many of the observed DEA processes can be satisfactorily explained within the simplified picture of a diatomic dissociation along a repulsive electronic state.[6–8]

Fairly recently it has been shown that low energy electrons can cause single and double strand breaks in plasmid DNA in the condensed phase.[9] As low energy electrons ($\leq$30 eV) are abundant along the track of ionizing radiation (5×10^5 MeV^{-1}),[10,11] this has significant consequences for our understanding of the damage such radiation causes in living organisms. Correspondingly, the focus of DEA studies in recent years has moved to more complex, biologically relevant molecules.[7,12] It has also become increasingly apparent that, besides the fast, direct dissociation processes commonly observed in DEA, rearrangement and further fragmentation on the metastable time scale can also play a significant role.[13–15] In DEA to the nucleobases and the amino acids, the dominating process is found to be hydrogen abstraction[15–17] and it has been shown that the dehydrogenation site is selective within a given resonance.[15,18,19] In this case, the initially formed TNI can be in an electronically excited state that relaxes to form $[M - H]^-$ in the electronic ground state but with sufficient internal energy to enable further fragmentation.

This scenario is in many ways comparable to the situation in UV-MALDI where the photon energy of the desorption laser

Science Institute and University of Iceland, Department of Chemistry, Dunhagi 3, 107 Reykjavík, Iceland. E-mail: odduring@hi.is
† Electronic supplementary information (ESI) available. See DOI: 10.1039/c1cp21298b

initially causes an electronic excitation, which is transformed into vibrational excitation and then to some extent to translational motion. The ionisation takes place through proton transfer under multiple collision conditions in the expanding plume and the ions have relaxed to their electronic ground state before metastable fragmentation takes place.[20–22] Previously, we have studied the metastable fragmentation of the amino acid valine after deprotonation at different deprotonation sites and compared the results with metastable decay of the same anions formed by hydrogen abstraction through DEA. In these studies, we could show that the metastable decay pathways are strongly dependent on the charge location after the hydrogen loss from the precursor ion but independent of its formation mechanism. That is, we found the fragmentation mechanism to be the same when the parent ion was formed through hydrogen abstraction in DEA and when it was formed through deprotonation in a proton transfer process. Furthermore, in our studies on valine, we used classical dynamics simulations to study the unimolecular decay processes. For this fairly simple molecule, our theoretical approach was quite successful and showed predictive value.[15]

Motivated by: (i) our success in the application of simulations as a predictive tool to study unimolecular decay processes, (ii) the potential role of unimolecular decay of negatively charged ions in radiation damage and (iii) the increasing significance of metastable decay processes in analytical mass spectrometry, we have extended our studies to more complex biologically relevant molecules. Here, we present measurements on the metastable fragmentation (200 ns–10 μs) of the deoxynucleosides and nucleosides constituting DNA and RNA. The deprotonated parent molecules were formed by means of matrix assisted laser desorption/ionisation (MALDI). The fragmentation was found to depend strongly on the site of deprotonation and in order to recognise the fragments resulting from each site and deduce the fragmentation pathways, we have systematically blocked the various deprotonation sites by chemical modification. The experimental results are compared with classical dynamics simulations of the fragmentation processes for the individual parent ions after they have been deprotonated at the various sites.

For $[M - H]^-$ fragments formed in DEA, the internal energy comprises the kinetic energy of the incident electron and the electron affinity of [M − H] less the M − H binding energy. In the MALDI process the excess energy comprises the total internal energy of the molecule acquired in the desorption/ionization process. In our simulations, we thus assume that the target molecules have relaxed to their electronic ground state before fragmentation takes place, but have considerable internal energy. Even for these rather large molecules, our simulations give results that correspond closely with the measurements.

Methods

Metastable decay measurements

Metastable decay of the respective deprotonated nucleosides and 2′-deoxynucleosides was measured in negative ion, post source decay (PSD) mode with a UV MALDI mass spectrometer (MALDI-MS) (Reflex IV, Bruker Daltonics, Bremen, Germany). The instrument and its operation has been described in detail elsewhere.[23] In brief, ions were generated in the MALDI process with an N_2-laser at 337 nm. The repetition rate was 7–10 Hz and the power was kept about 20% above the detection threshold for the corresponding ions. To average out sample inhomogeneity the laser spot was moved manually over the sample during acquisition. Negative ions were extracted in pulsed delayed extraction mode with a delay time of 200 ns and accelerated into a reflectron time-of-flight (ToF) mass spectrometer. The PSD spectra were recorded by gating selective parent ions into the field free linear region of the mass spectrometer. The mass gate was set at ±5 Da in all experiments. The total acceleration voltage into the field free linear region was 25 kV resulting in about 10 μs flight time. The time window within which we observe metastable decay is thus from about 200 ns to about 10 μs. Hence from the time point the ions leave the acceleration region until they reach the end of the linear flight tube. After the linear flight the ions were decelerated and reaccelerated with a gridless reflectron and detected with a double micro-channel plate detector. The reflectron voltage was stepped down in 9 segments to assure for collection of all fragments. Individual segments are the sum of 500 shots, which were recorded by using the fragmentation analyses and structural ToF method FAST, within the instrumental control software FlexControl®. The alignment of individual segments and the mass calibration of the spectra were carried out with the FlexAnalyses® software also provided by the instrument manufacturer.

The sample molecules guanosine, uridine, adenosine, cytidine, 2′-deoxy guanosine, 2′-deoxy adenosine, 2′-deoxy cytidine and 2′-deoxy thymidine were acquired from Sigma-Aldrich, Germany as high purity samples (> 98%) and used without further purification. The modified uridines; *N*-methyl uridine, 2′,3′-*O*-isopropylidene uridine, 2′,3′-*O*-isopropylidene, 5′-*O*-methyl uridine and 2′,3′-*O*-isopropylidene *N*-methyl uridine and the modified guanosines; *N*-methyl guanosine, 2′,3′-*O*-isopropylidene guanosine, and 2′,3′-*O*-isopropylidene 5′-*O*-methyl guanosine were prepared in-house from the respective nucleosides. The preparation and purification protocols are described in ESI.†

Samples were prepared by co-spotting 0.5 μL of a 1 mg mL^{-1} aqueous solution of the matrix bisbenzimide hydrochloride; $C_{25}H_{24}N_6O{\cdot}3HCl$ (≥ 98%, Sigma-Aldrich, Germany) and 0.5 μL of a 10 mg mL^{-1} solution of the nucleoside samples in methanol on a stainless steel sample carrier.

Classical dynamics simulations

The calculations were carried out using density functional theory (DFT) with a plane wave basis set (energy cut-off at 395.994 eV) and the PW91 functional as implemented in the VASP code.[24,25] The plane wave basis set is convenient to use in classical dynamics simulations because all parts of the simulation box are equally well represented and the basis functions do not change as the atoms move. This, however, means that periodic boundary conditions are enforced. The box length was chosen to be 18 Å and the interactions between periodic images should therefore be negligible. The total

charge of the simulated system has to be zero in this approach, so a uniform compensating background is introduced when the ions are simulated. The uniform background does not affect the forces acting on the atoms and therefore does not affect the dynamical simulations.

First, the molecular geometry was optimized to find the minimum energy structure for each molecule. The minimization was carried out by first using damped molecular dynamics and then, after the force had become smaller than 0.3 Å eV^{-1}, conjugate gradient algorithm. The same was done for the deprotonated ions to estimate their stability. To account for thermal distortions in the initial, room temperature samples, the energy minimum configuration of the neutral compound was given internal energy corresponding to a temperature of 298 K by scaling the atom velocities. The vibrational modes were allowed to equilibrate in a dynamics simulation covering 1000 fs. After equilibration, the dynamics were simulated for additional 1000 fs to create a set of 10 configurations separated by a time interval of 100 fs.

The individual configurations were used as starting points for the further simulations of the fragmentation processes. To account for the excitation energy acquired by the molecule during the MALDI process, the atomic velocities of the individual configurations were scaled to correspond to a total of 8 eV internal energy. Also, a selected proton was removed from the molecules. Then, a constant energy (microcanonical) simulation of the highly vibrationally excited, deprotonated ions in their ground electronic state was carried out for 500 fs. The dissociations which occurred during this simulation period were documented and the charge of each fragment was determined by Bader's method.[26–28] These simulations are only a rough representation of the experimental conditions and the internal energy added (8 eV) is higher than what has been estimated for small molecules in MALDI, 4–5 eV.[29,30] In our measurements, the observation time after mass selection is about 10 μs. The computational effort for such long trajectories is excessive. The higher internal energy is chosen to accelerate the fragmentation so that it can be observed in much shorter trajectories. However, it is important to be aware that increasing the internal energy may also open new fragmentation channels and change the ratio between different channels.

To elucidate the fragmentation mechanisms responsible for the metastable dissociation of the deprotonated anions, and to test the ability of the simulation approach to predict fragmentation products, we simulated the dynamics of uridine and 2′-deoxy guanosine after deprotonation at the various sites. The uridine is a pyrimidine base and a ribose sugar while 2′-deoxy guanosine is a purine base and a 2′-deoxyribose sugar unit. Hence, with these two model systems we include the four different principal components that make up DNA and RNA.

Results and discussion

Mass spectra of metastable decay products

Fig. 1 shows the metastable decay spectra for the deprotonated nucleosides adenosine (A), guanosine (G), cytidine (C) and uridine (U). For the native purine containing nucleosides A and G the only operative channels are the glycosidic bond rupture leading to the observation of the deprotonated base $[B–H]^-$, and a $^{0,2}X$ cross ring cleavage of the sugar leading to the fragment $[B + 42]^-$ ($^{0,2}X$ cross ring cleavage and the complementary $^{0,2}A$ cross ring cleavage are depicted in Fig. 3, for further detail on the nomenclature for the sugar cross ring cleavage see ref. 31). In addition to these channels the pyrimidines show a specific fragmentation channel, that is driven by the formation of NCO^- or the loss of neutral HNCO from the deprotonated parent ion. In cytidine, the charge retention is primarily on the high electron affinity fragment NCO (EA = 3.6 eV[32]) and the cyanate anion formation dominates. In uridine, on the other hand, the formation probability of NCO^- and the complementary anion $[(M – H)–HNCO]^-$ are comparable. Furthermore, the glycosidic bond rupture in uridine also partly leads to charge retention on the ribose unit resulting in the observation of the fragment $[R–H]^-$. Additional masses that are not observed from the other nucleosides are observed from cytidine at *m/z* 138, 174 and 182. We assign these to the fragments $[C_4H_8O_3]^-$ ($^{1,5}X$ sugar cross ring cleavage), $[M – C_3H_4N_2]^-$ (base fragmentation) and $[M – C_2H_4O_2]^-$ ($^{0,3}X$ sugar cross ring cleavage), respectively.

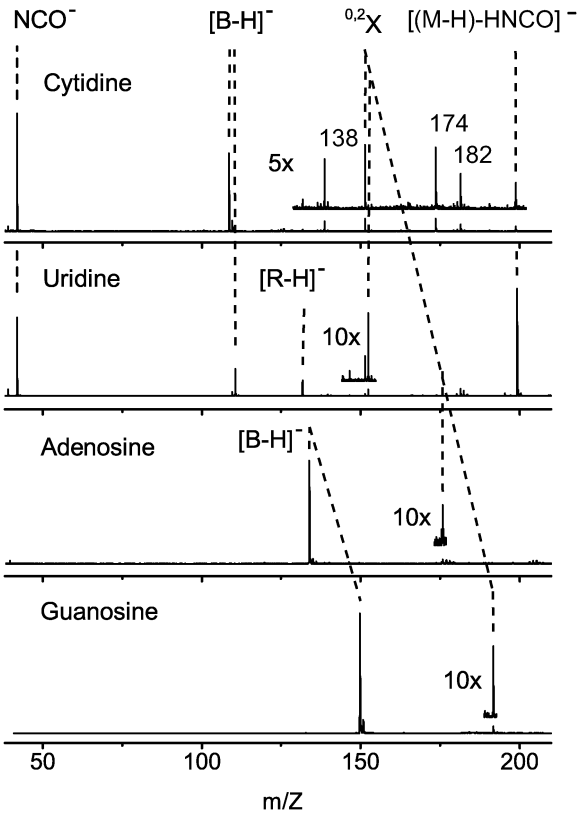

Fig. 1 Fragmentation mass spectra of nucleosides. All main fragmentations are labelled and those in common for more than one nucleoside are connected by dotted lines. A glycosidic bond rupture creating the anion $[B–H]^-$ and an $^{0,2}X$ sugar cross ring cleavage creating $[B + 42]^-$ are observed from all four nucleosides, while NCO^- and $[(M – H)–HNCO]^-$ are observed from pyrimidines only.

Fig. 2 shows the metastable decay spectra for the deprotonated 2′-deoxynucleosides deoxyadenosine (dA), deoxyguanosine (dG), deoxycytidine (dC) and thymidine (T). Compared to the corresponding nucleosides the 2′-deoxynucleosides have

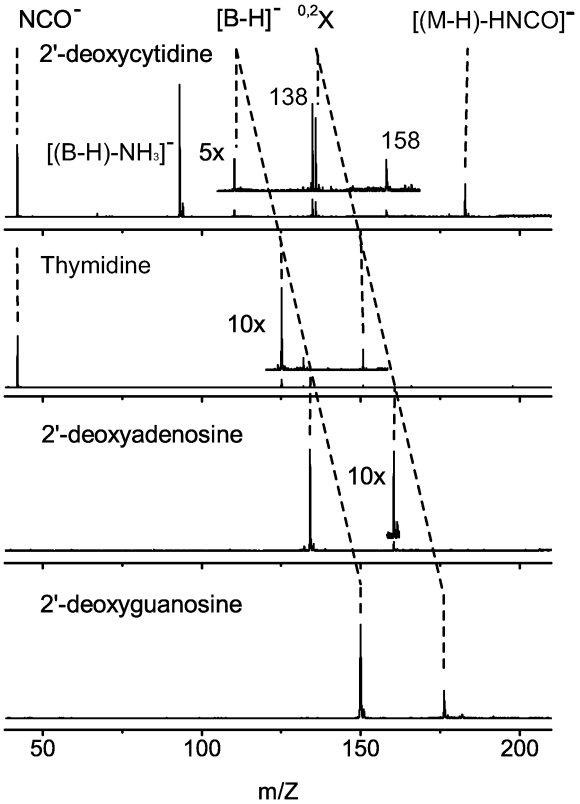

Fig. 2 Fragmentation mass spectra of 2′-deoxynucleosides. All main fragments are labelled and these in common for more than one 2′-deoxynucleoside are connected by dotted lines. A glycosidic bond rupture creating $[B–H]^-$ and a $^{0,2}X$ sugar cross ring cleavage creating $[B + 26]^-$ are observed from all four 2′-deoxynucleosides, while NCO^- and $[(M - H)–HNCO]^-$ are observed from pyrimidines only.

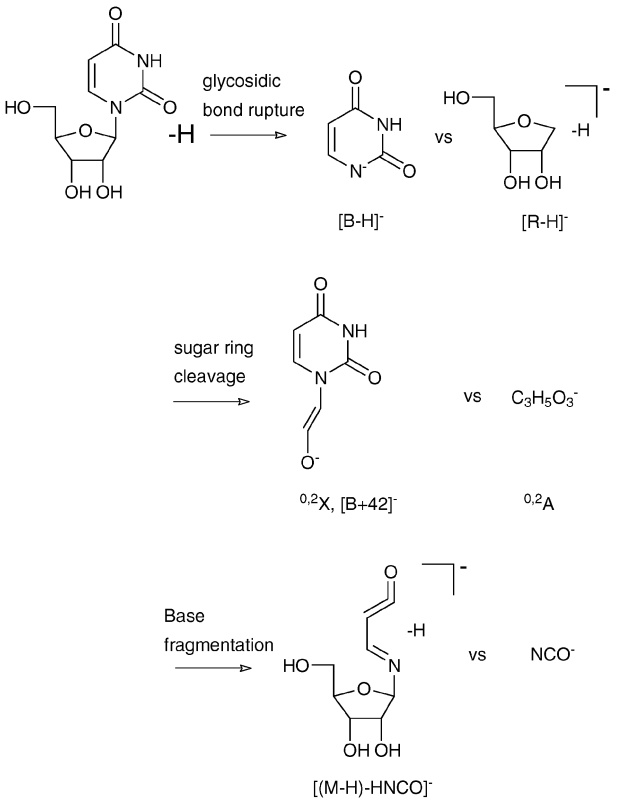

Fig. 3 The main fragmentation observed for the nucleosides and 2′-deoxynucleosides depicted as an example of uridine. The bond ruptures are identical for all nucleosides and 2′-deoxynucleosides, but base fragmentation is only observed from pyrimidine nucleosides and 2′-deoxynucleosides.

one hydroxyl group less, *i.e.* one deprotonation site has been removed from the sugar moiety. Nonetheless, the 2′-deoxynucleosides show very similar fragmentation patterns as the ribonucleosides. A glycosidic bond rupture with charge retention on the base is observed in all 2′-deoxynucleosides, as well as a $^{0,2}X$ cross ring cleavage of the 2′-deoxyribofuranose ring, leading to the fragment $[B + 26]^-$. Like the pyrimidine-containing nucleosides, the pyrimidine-containing 2′-deoxynucleosides also show the formation of NCO^- and a loss of neutral HNCO from the deprotonated parent ion. Here, the formation of NCO^- dominates for thymidine as was the case for cytidine in the nucleosides. Similar to cytidine, 2′-deoxycytidine also shows more fragmentation than the other 2′-deoxynucleosides. Here NH_3 loss from the deprotonated base is prominent but also the masses 138 and 158 amu, corresponding to the fragments $[M - C_4H_8O_2]^-$ ($^{1,5}X$ sugar cross ring cleavage) and $[M - C_3H_4N_2]^-$ (base fragmentation), respectively, are observed. These fragmentations are identical to those observed for cytidine. Fig. 3 summarizes the main fragmentation channels common to the nucleosides and the deoxynucleosides.

Each nucleoside has several acidic protons, hence several different deprotonation sites that all potentially lead to distinct anions with different characteristics. These anions will in turn show different fragmentation patterns on the metastable time scale if they contain sufficient internal energy.

To clarify the role of individual deprotonation sites and how they lead to the characteristic fragmentation patterns of the purine- and pyrimidine-containing nucleosides, we have modified the nucleosides uridine and guanosine to selectively block individual deprotonation sites. Hence, by blocking a deprotonation site, the fragmentation channels, originating from the ion created by deprotonation from that site, are quenched and thus the relation between the fragmentation channels and the deprotonation site can be identified. Fig. 4 shows the individual uridine and guanosine derivatives; *N*-methyl uridine **1** and *N*-methyl guanosine **5**, where the deprotonation of the nucleobase is blocked, 2′,3′-*O*-isopropylidene uridine **2** and 2′,3′-*O*-isopropylidene guanosine **6**, where the 2′-OH and 3′-OH deprotonation sites of the sugar moiety are blocked, 2′,3′-*O*-isopropylidene 5′-*O*-methyl uridine **3** and 2′,3′-*O*-isopropylidene 5′-*O*-methyl guanosine **7**, where all the sugar deprotonation sites are blocked, leaving only the nucleobase to deprotonate and 2′,3′-*O*-isopropylidene *N*-methyl uridine **4**, where all deprotonation sites except the 5′-OH group on the sugar are blocked.

Fig. 5 compares the metastable decay spectra of the native uridine to that of the **1**–**3** uridine analogues. 2′,3′-*O*-isopropylidene *N*-methyl uridine **4**, did not ionize by deprotonation from the 5′-OH, but ionized through demethylation. Its metastable decay spectra were thus not measured.

In **1** (Fig. 5b), where only the deprotonation of the base is blocked, the base fragmentation is quenched while the

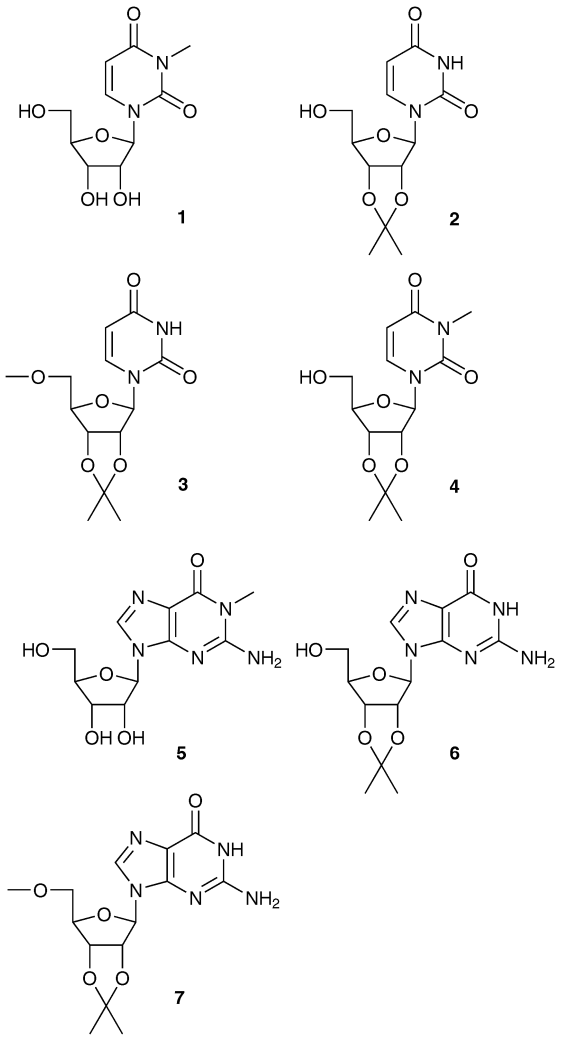

Fig. 4 Molecular structure of the modified uridines; *N*-methyl uridine, (**1**); 2′,3′-*O*-isopropylidene uridine, (**2**); 2′,3′-*O*-isopropylidene, 5′-*O*-methyl uridine, (**3**); 2′,3′-*O*-isopropylidene *N*-methyl uridine, (**4**); and the modified guanosines; *N*-methyl guanosine, (**5**); 2′,3′-*O*-isopropylidene guanosine, (**6**); and 2′,3′-*O*-isopropylidene 5′-*O*-methyl guanosine, (**7**). See ESI† for synthesis.

glycosidic bond rupture and sugar ring rupture remain intact. Additionally an elimination of the methyl group is observed. In **2** (Fig. 5c), and **3** (Fig. 5d) where deprotonation from the 2′- and 3′-, and the 2′-, 3′-, and 5′-hydroxyl groups on the sugar are blocked, respectively, the glycosidic bond rupture and the sugar cross ring cleavage, is quantitatively quenched. Here, the fragment mass spectra consist of NCO^- and loss of HNCO through base fragmentation. This is independent of whether the 5′-hydroxyl group is blocked or not. In addition to these fragmentation channels, a loss of $(CH_3)_2CO$ from the isopropylidene protective group was observed from **2** and **3** (unlabeled peaks in panels (c) and (d)). This was confirmed by using fully deuterated isopropylidene as protection group.

In summary, the spectra show that the base fragmentation proceeds exclusively through deprotonation on the base while the glycosidic bond rupture and sugar cross ring cleavage are due to deprotonation of the 2′-OH or the 3′-OH group of the sugar moiety.

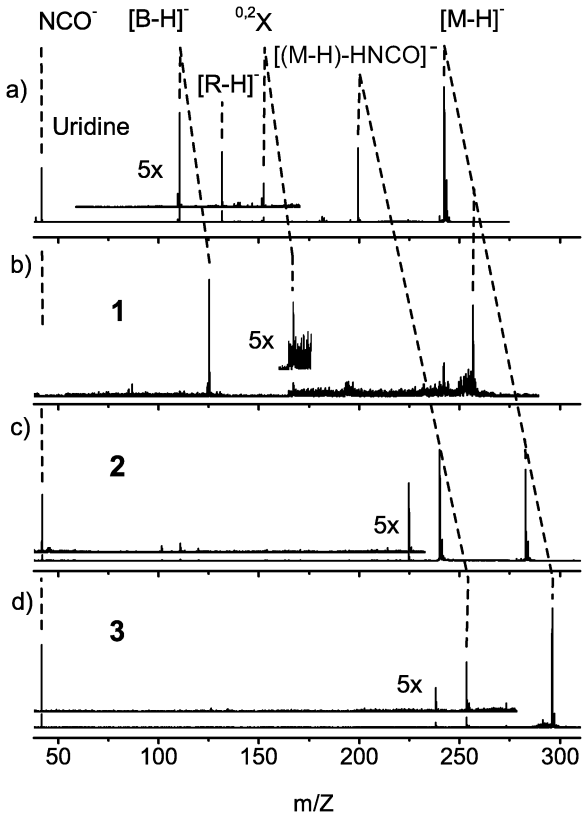

Fig. 5 Fragmentation mass spectra of native and modified uridine: (a) native uridine, (b) **1** where deprotonation at the base is blocked, (c) and (d), **2** and **3**, respectively, where deprotonation at the sugar is blocked. Glycosidic bond rupture and $^{0,2}X$ sugar cross ring cleavage are observed upon sugar deprotonation (panel b). Base fragmentation resulting in NCO^- and the fragment $[(M - H)–HNCO]^-$ are observed upon base deprotonation (panels c and d).

Fig. 6 compares the metastable decay spectra of the native guanosine to that of the guanosine derivatives **5–7**. The results are virtually the same as for uridine, hence blocking the base deprotonation site does not influence the glycosidic bond rupture nor does it influence the $^{0,2}X$ cross ring cleavage of the sugar moiety. However, these channels are close to be quantitatively quenched by blocking the 2′- and 3′-hydroxyl groups on the sugar (The low intensity residual signal at *m*/*z* 150 in panels b–d in Fig. 6 is attributed to residual native guanosine impurities in the in-house prepared derivatives **5–7**.). Similar to the uracil we can conclude that for guanosine: (i) the nucleobase deprotonation does not lead to further fragmentation (this reflects the fact that we do not observe any base fragmentation from the metastable decay of deprotonated purine containing nucleosides) and (ii) the sugar deprotonation leads to glycosidic bond rupture as well as a $^{0,2}X$ cross ring rupture of the sugar.

Simulations of the metastable decay process

With the assumptions and approximations discussed in the methods section on classical dynamic simulations, we have simulated the unimolecular fragmentation of the $[M - H]^-$ ions that are possibly formed by deprotonation of uridine

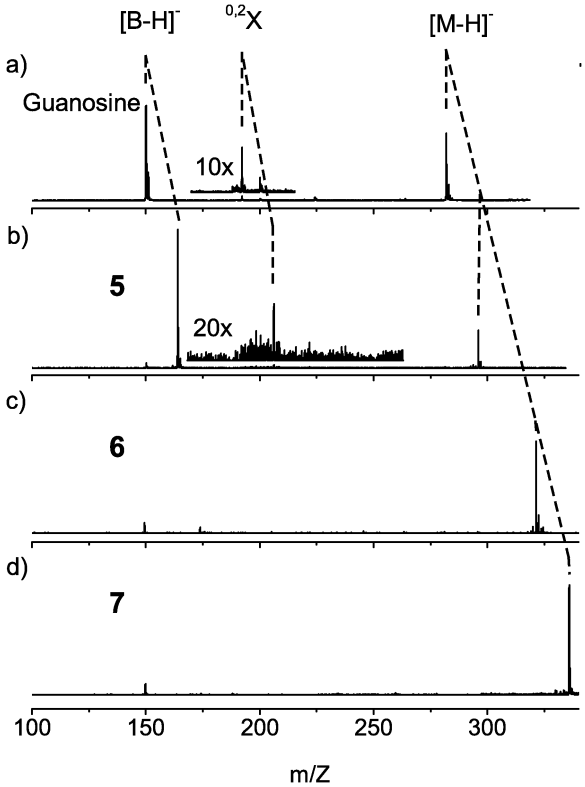

Fig. 6 Fragmentation mass spectra of native and modified guanosine: (a) native guanosine, (b) **5**, where deprotonation at the base is blocked, (c) and (d), **6** and **7**, respectively, where deprotonation at the sugar is blocked. Glycosidic bond rupture and ^{0,2}X sugar cross ring cleavage are observed upon sugar deprotonation (panel b). Base deprotonation does not lead to further fragmentation of the purines (panels c and d).

and 2′-deoxyguanosine. For uridine, we have compared removing a proton from (i) the N3 at the base, (ii) the 2′-OH of the sugar and (iii) the 3′-OH of the sugar. For 2′-deoxyguanosine we simulated the fragmentation of the anions formed by removing a proton from (i) N1 at the base, (ii) the primary amine group at C2 of the base, (iii) C8 at the base and (iv) the 3′-OH of the sugar.

A minimum was not found for 5′-OH deprotonated uridine during the geometry optimization, it spontaneously transformed to 3′-OH deprotonated uridine, which is consistent with our experimental findings that **4** did not ionize through deprotonation of the 5′-OH group. Thus, simulations of decay after 5′-OH deprotonation were not carried out.

Fig. 7 shows snapshots from the simulations along with a representation of the observed fragmentation mechanism for uridine when the proton is removed from (a) the N3 at the base, (b) the 2′-OH and (c) the 3′-OH of the sugar. A proton removal from the 2′-OH is identical to a proton removal from 3′-OH, as the 1,2-diol arrangement allows for low-energy barrier proton sharing between the two hydroxyl groups. This barrier has been estimated to be 2.91 kcal mol^{-1} and gets reduced to 0.59 kcal mol^{-1} when the zero point energy correction is made.[33] It is, therefore, negligible compared to the internal energy of the molecules in our simulations, as well as in the experiments.

In simulations of uridine deprotonated from N3, three out of ten (3/10) simulations lead to base fragmentation through NCO^- excision and no other fragmentation channels were observed. This is in very good agreement with our experimental observations except for the fact that in the simulation the charge remains exclusively on the high electron affinity fragment NCO, and the ion $[(M - H)–HNCO]^-$, which is complementary with regards to the retention of one proton, is not observed. Proton removal from the 2′-OH or the 3′-OH, on the other hand, leads to a glycosidic bond rupture in thirteen out of twenty (13/20) simulations *via* three different fragmentation mechanisms originating equally from the deprotonated 2′-OH and 3′-OH. One of these mechanisms is shown in Fig. 7b. A ^{0,2}A cross ring cleavage of the sugar was observed in two out of twenty (2/20) simulations (Fig. 7c). This is again in very good agreement with our experimental observations except for the fact that the cross ring cleavage of the sugar in our simulation leads to charge retention on the A fragment, whereas in our experiments, the charge retention is on the X fragment. Furthermore, in our experiments, the glycosidic bond rupture was found to lead to charge retention on the sugar moiety as well as on the base.

Fig. 8 shows snapshots from the simulations of the fragmentation of 2′-deoxyguanosine when it is deprotonated at the 3′-OH along with a representation of the observed fragmentation mechanism. In four out of ten (4/10) simulations, deprotonation at the 3′-OH leads to glycosidic bond rupture with charge retention on the base and in two out of ten (2/10) simulations, deprotonation at the 3′-OH leads to a ^{0,2}A sugar cross ring cleavage. These are the same fragmentation channels observed in our experiments, but again the charge retention in the cross ring cleavage of the sugar is on the complementary fragment: ^{0,2}A, compared to ^{0,2}X in our experiments. A statistical decay orients the fragmentation path towards the energetically lowest state available, or in some cases two different states if the energy difference is small. An energy minimization shows that the ^{0,2}X fragment is approximately 0.74 eV lower in energy than the ^{0,2}A fragment, confirming that the charge retention in our experiments is on the energetically more favourable fragment.

In our simulations of the fragmentation of 2′-deoxyguanosine, none of the ions deprotonated at the base lead to further fragmentation during the time interval simulated, which agrees with the measurements.

Conclusions

The experimental results show a clear fragmentation pattern, for all the nucleosides, which depends on the nature of the base, *i.e.* if it is a purine or pyrimidine base. Furthermore, by blocking individual deprotonation sites we were able to determine which deprotonation sites are responsible for the individual fragments. For the purine bases, the only operative channels are the glycosidic bond rupture leading to the fragment $[B–H]^-$, and a ^{0,2}X cross ring cleavage leading to the fragment $[B + 42]^-$. For the pyrimidine containing nucleosides both of these channels are also operative and additionally we observe base fragmentation leading to the formation of NCO^- and $[(M - H)–HNCO]^-$. By blocking individual deprotonation sites we have unambiguously

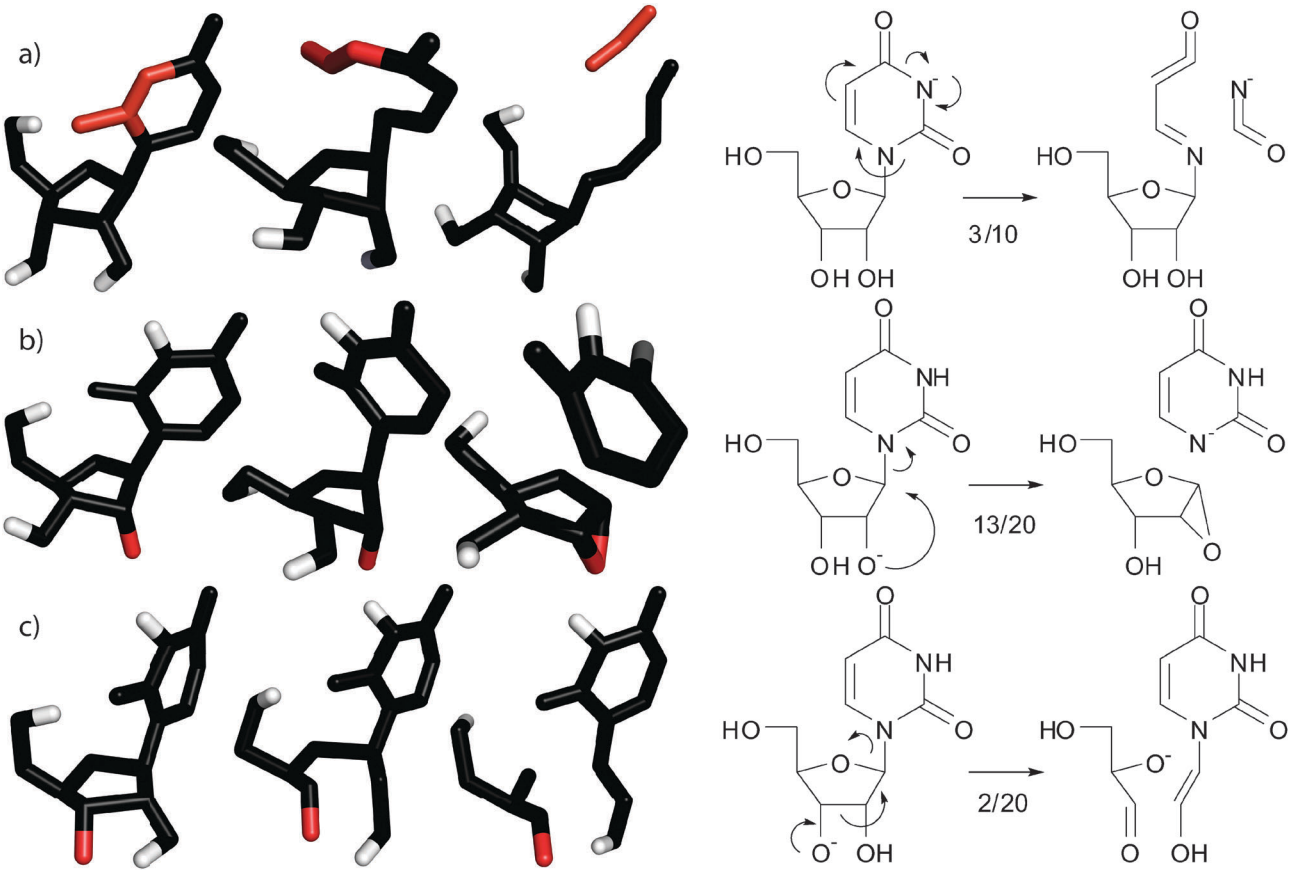

Fig. 7 Snapshots from classical dynamics simulations of deprotonated uridine on the left, on the right the observed mechanisms are depicted. The acidic protons are shown in white, the site of deprotonation in gray and the neutral atoms in black. The ratios under the arrows indicate the number of trajectories, which result in the fragmentation depicted over the number of simulations. Three fragmentation channels are observed; (a) NCO^- formation after deprotonation at 3N of the base, (b) glycosidic bond rupture after 2′- or 3′-OH deprotonation of the sugar, (c) ^{0,2}A sugar cross ring cleavage after 2′- or 3′-OH deprotonation of the sugar. The 2′- and 3′-OH deprotonation are indistinguishable in our experiments.

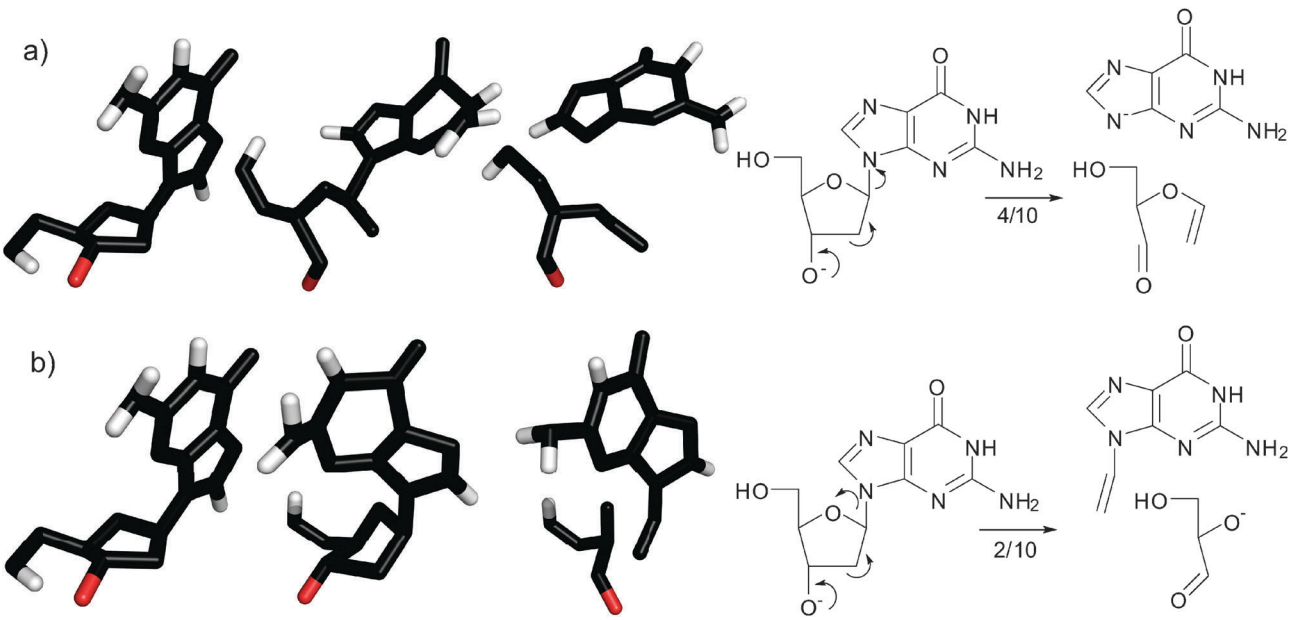

Fig. 8 Snapshots from classical dynamics simulations of deprotonated 2′-deoxyguanosine on the left, on the right the observed mechanism is depicted. The acidic protons are shown in white, the deprotonation site in gray and the neutral atoms in black. The ratios under the arrows indicate the number of trajectories, which result in the fragmentation depicted over the number of simulations. For 2′-deoxyguanosine two fragmentation channels are observed; (a) glycosidic bond rupture and (b) ^{0,2}A cross ring cleavage. Both of these channels result from 2′- or 3′-OH sugar deprotonation. Simulations of base deprotonation did not result in further fragmentation.

shown that base fragmentation proceeds exclusively from a precursor that is deprotonated at N3 of the base in the pyrimidines but is not operative in the purines. The glycosidic bond rupture and the cross ring cleavage of the sugar, on the other hand, proceeds exclusively from a precursor that is deprotonated at the 2′ or 3′ positions of the sugar. Due to the low proton transfer barrier between these deprotonation sites they are indistinguishable in our experiments.

Our simulations reproduce the observed bond ruptures accurately. A simulated fragmentation of uridine deprotonated at the N3 of the base shows a base fragmentation leading to the formation of NCO^- and no other fragmentation. Simulated fragmentation of uridine deprotonation at the 2′-OH or the 3′-OH of the sugar, on the other hand results in predominant glycosidic bond rupture but also in sugar cross ring cleavage. In the simulations of the fragmentation of deprotonated 2′-deoxyguanosine, we also find excellent agreement with our experimental results with regards to the bond ruptures. A deprotonation at the base does not lead to further fragmentation despite the relatively high internal energy ascribed to the molecule. Deprotonation at the 3′-positions of the sugar, on the other hand, results in glycosidic bond rupture as well as in sugar cross ring cleavage. The results from our simulations are very promising with regards to the predictability of the position of the bond ruptures. However, the charge retention is often not correctly reproduced. For the cross ring cleavage, we exclusively observe the formation of the ^{0,2}A fragment in our simulations, but we only observe the complementary ^{0,2}X fragments in our experiments. The simulated charge retention for the glycosidic bond rupture and the base fragmentation is also not in agreement with the measurements. This shortcoming of our simulations is probably due to the semi-local functional approximation used (PW91). It is well known that such functionals do not describe charge localization effects well.[34–36] Currently, we are improving the simulation methodology by including self-interaction correction, which gives more accurate energetics and charge distribution. Nevertheless, considering the complexity of these systems, the overall agreement between the simulations presented here and experiments is quite good.

Acknowledgements

This work was supported by the Icelandic Centre for Research (RANNIS) and by the University of Iceland Research Fund. HDF acknowledges a PhD grant from the Eimskip University Fund. This work was conducted within the framework of the COST Action CM0601 (ECCL).

References

1 D. Chandler, *J. Stat. Phys.*, 1986, **42**, 49–67.
2 P. B. Armentrout and T. Baer, *J. Phys. Chem.*, 1996, **100**, 12866–12877.
3 T. Baer and W. L. Hase, *Unimolecular Reaction Dynamics, Theory and Experiments*, Oxford University Press, New York, 1996.
4 J. B. Fenn, M. Mann, C. K. Meng, S. F. Wong and C. M. Whitehouse, *Science*, 1989, **246**, 64–71.
5 J. Wu and S. A. McLuckey, *Int. J. Mass Spectrom.*, 2004, **237**, 197–241.
6 O. Ingólfsson, F. Weik and E. Illenberger, *Int. Rev. Phys. Chem.*, 1996, **15**, 133–151.
7 I. Bald, J. Langer, P. Tegeder and O. Ingólfsson, *Int. J. Mass Spectrom.*, 2008, **277**, 4–25.
8 E. Illenberger and J. Momigny, *Gaseous Molecular Ions. An Introduction to Elementary Processes Induced by Ionization*, Steinkopff Verlag, Springer-Verlag, Darmstadt, New York, 1992.
9 B. Boudaiffa, P. Cloutier, D. Hunting, M. A. Huels and L. Sanche, *Science*, 2000, **287**, 1658–1660.
10 S. M. Pimblott and J. A. LaVerne, *Radiat. Phys. Chem.*, 2007, **76**, 1244–1247.
11 ICRU, *International Commission on Radiation Units and Measurements*, 1979.
12 L. Sanche, *Eur. Phys. J. D*, 2005, **35**, 367–390.
13 F. Zappa, M. Beikircher, A. Mauracher, S. Denifl, M. Probst, N. Injan, J. Limtrakul, A. Bacher, O. Echt, T. D. Märk, P. Scheier, T. A. Field and K. Graupner, *ChemPhysChem*, 2008, **9**, 607–611.
14 R. D. Leib, W. A. Donald, M. F. Bush, J. T. O'Brien and E. R. Williams, *J. Am. Soc. Mass Spectrom.*, 2007, **18**, 1217–1231.
15 H. D. Flosadóttir, S. Denifl, F. Zappa, N. Wendt, A. Mauracher, A. Bacher, H. Jónsson, T. D. Maerk, P. Scheier and O. Ingólfsson, *Angew. Chem., Int. Ed.*, 2007, **46**, 8057–8059.
16 S. Denifl, S. Ptasinska, M. Probst, J. Hrusak, P. Scheier and T. D. Märk, *J. Phys. Chem. A*, 2004, **108**, 6562–6569.
17 H. Abdoul-Carime, J. Langer, M. A. Huels and E. Illenberger, *Eur. Phys. J. D*, 2005, **35**, 399–404.
18 S. Ptasinska, S. Denifl, P. Scheier, E. Illenberger and T. Märk, *Angew. Chem., Int. Ed.*, 2005, **44**, 6941–6943.
19 S. Ptasinska, S. Denifl, V. Grill, T. D. Märk, E. Illenberger and P. Scheier, *Phys. Rev. Lett.*, 2005, **95**, 4.
20 R. Knochenmuss, *Analyst*, 2006, **131**, 966–986.
21 R. Knochenmuss and R. Zenobi, *Chem. Rev.*, 2003, **103**, 441–452.
22 R. Zenobi and R. Knochenmuss, *Mass Spectrom. Rev.*, 1998, **17**, 337–366.
23 M. Stano, H. D. Flosadóttir and O. Ingólfsson, *Rapid Commun. Mass Spectrom.*, 2006, **20**, 3498–3502.
24 G. Kresse and J. Furthmuller, *Phys. Rev. B: Condens. Matter*, 1996, **54**, 11169–11186.
25 G. Kresse and J. Hafner, *Phys. Rev. B: Condens. Matter*, 1994, **49**, 14251–14269.
26 G. Henkelman, A. Arnaldsson and H. Jónsson, *Comput. Mater. Sci.*, 2006, **36**, 354–360.
27 E. Sanville, S. D. Kenny, R. Smith and G. Henkelman, *J. Comput. Chem.*, 2007, **28**, 899–908.
28 W. Tang, E. Sanville and G. Henkelman, *J. Phys.: Condens. Matter*, 2009, **21**, 084204.
29 V. Gabelica, E. Schulz and M. Karas, *J. Mass Spectrom.*, 2004, **39**, 579–593.
30 G. H. Luo, I. Marginean and A. Vertes, *Anal. Chem.*, 2002, **74**, 6185–6190.
31 B. Domon and C. E. Costello, *Glycoconjugate J.*, 1988, **5**, 397–409.
32 S. E. Bradforth, E. H. Kim, D. W. Arnold and D. M. Neumark, *J. Chem. Phys.*, 1993, **98**, 800–810.
33 E. Bosch, M. Moreno and J. M. Lluch, *Can. J. Chem.*, 1992, **70**, 1640–1644.
34 J. Laegsgaard and K. Stokbro, *Phys. Rev. Lett.*, 2001, **86**, 2834–2837.
35 G. Pacchioni, F. Frigoli, D. Ricci and J. A. Weil, *Phys. Rev. B: Condens. Matter*, 2001, **63**, 8.
36 H. Jónsson, *Proc. Natl. Acad. Sci. U. S. A.*, 2011, **108**, 944–949.

